26. Well completion is the process to ready for injection. This process includes installing tubing used to inject fluid, perforating the portion of the well in the injection zone, and casing the well to ensure no injection fluids leakage.
27. K. E. Murray, A. A. Holland, *Shale Shaker* **65**, 98–106 (2014).
28. C. Frohlich, J. I. Walter, J. F. W. Gale, *Seismol. Res. Lett.* **86** (2A), 492–499 (2015).
29. A. McGarr, *J. Geophys. Res.* **81**, 1487–1494 (1976).
30. A. McGarr, *J. Geophys. Res.* **119**, 1008–1019 (2014).
31. L. V. Block, C. K. Wood, W. L. Yeck, V. M. King, *Seismol. Res. Lett.* **85**, 609–624 (2014).
32. Y. Zhang *et al.*, *Ground Water* **51**, 525–538 (2013).
33. The volume conversion from the oil industry standard of barrels to the metric standard of meters cubed is ~6.29 barrels per meter cubed, assuming a 42-gallon oil barrel.
34. B. Efron, R. J. Tibshirani, *An Introduction to the Bootstrap* (CRC press, Boca Raton, FL, 1994).
35. Information on materials and methods is available on *Science* Online.
36. J. Rutqvist *et al.*, *Math. Geosci.* **47**, 3–29 (2015).
37. W. D. Mooney, M. K. Kaban, *J. Geophys. Res.* **115**, B12424 (2010).

ACKNOWLEDGMENTS

This work was conducted as a part of the Understanding Fluid Injection Induced Seismicity Project supported by the John Wesley Powell Center for Analysis and Synthesis, funded by the U.S. Geological Survey (grant G13AC00023). We thank J. Hardebeck and W. Ellsworth for their thoughtful comments. This project was aided by injection data contributed by A. Holland (OK), C. Eisenger (CO), T. Kropatsch (WY), J. Amrheim (IN), T. Tomastik (OH), S. Platt (PA), I. Allred (UT), M. Berry (UT), A. Wickert (TX), and I. Van-Vloten (CEUS). This project used earthquake data from the ANSS Comprehensive Catalog. The well data used in this study are available as supplementary materials on *Science* Online.

SUPPLEMENTARY MATERIALS

www.sciencemag.org/content/348/6241/1336/suppl/DC1
Materials and Methods
Figs. S1 to S18
Tables S1 to S4
References (*38*–*46*)

16 March 2015; accepted 28 May 2015
10.1126/science.aab1345

POLARON DYNAMICS

Long-lived photoinduced polaron formation in conjugated polyelectrolyte-fullerene assemblies

Rachel C. Huber,[1]* Amy S. Ferreira,[1]* Robert Thompson,[1] Daniel Kilbride,[1] Nicholas S. Knutson,[1] Lekshmi Sudha Devi,[1] Daniel B. Toso,[2] J. Reddy Challa,[1] Z. Hong Zhou,[2,3] Yves Rubin,[1]† Benjamin J. Schwartz,[1,3]† Sarah H. Tolbert[1,3,4]†

The efficiency of biological photosynthesis results from the exquisite organization of photoactive elements that promote rapid movement of charge carriers out of a critical recombination range. If synthetic organic photovoltaic materials could mimic this assembly, charge separation and collection could be markedly enhanced. We show that micelle-forming cationic semiconducting polymers can coassemble in water with cationic fullerene derivatives to create photoinduced electron-transfer cascades that lead to exceptionally long-lived polarons. The stability of the polarons depends on the organization of the polymer-fullerene assembly. Properly designed assemblies can produce separated polaronic charges that are stable for days or weeks in aqueous solution.

In biological photosynthetic systems, energy cascade structures promote the spatial separation of photogenerated charges created at the reaction center, preventing their recombination. These energy cascade structures require close proximity of the electron donors and acceptors, on the scale of ~1 nm, and the corresponding electron transfer (ET) processes take only a few picoseconds (*1*). Similarly, photoexcitation in artificial organic photovoltaic (OPV) cells generates dissociated charges at a donor-acceptor interface on subpicosecond time scales. However, OPVs suffer a large degree of recombination because they rely on phase separation of the conjugated polymer donor and fullerene acceptor into domains on the length scale of 10 to 20 nm to facilitate efficient exciton diffusion and charge transfer (*2*, *3*). The high charge densities present in OPVs, coupled with the low dielectric constant of organic materials, favor carrier recombination before the charges can be extracted through external electrodes. If OPVs could be designed to use ET cascade structures that are reminiscent of photosynthetic complexes, it should be possible to greatly improve charge separation and reduce recombination losses (*4*).

Here we describe how molecular self-assembly can enable dissolved OPV materials (conjugated polymers and fullerenes) in aqueous solution to mimic the ET cascade structures of biological complexes and allow us to "spatially" control photogenerated charges. We demonstrate efficient long-time charge separation following photoexcitation: The ET cascade produces separated polarons that are exceptionally stable for weeks, a lifetime that is unprecedented for OPV materials. Although long polaron lifetimes have been observed in covalently linked donor-acceptor dyads and triads (*5*) and micellar structures (*6*), our use of standard organic photovoltaic materials sets this work apart. In addition, our use of self-assembly provides potential future advantages in reproducibility and scalability, both of which are major hurdles for conventional OPVs with kinetically controlled structures (*7*–*9*). Finally, the photoinduced charge separation we achieve takes place in water, opening possibilities for the "green" production of artificial photosynthetic devices.

The particular materials used in this study are a combination of a conjugated polyelectrolyte, poly(fluorene-alt-thiophene) (PFT) (*10*), and several regioisomers of the charged fullerene derivatives C_{60}-*N*,*N*-dimethylpyrrolidinium iodide [$C_{60}(PI)_n$], where n is the number of charged pyrrolidinium iodide groups (*11*) (Fig. 1, A to C). PFT is a water-soluble semiconducting polyelectrolyte whose bis-alkylated sp^3-hybridized fluorenyl carbon forms a wedge-shaped monomer that facilitates the assembly of the charged polymer into rod-like micelles (Fig. 1B); details of how this polymer assembles have been published previously (*10*). Because of the charged nature of the polymer, the electron acceptor(s) must also carry cationic charges to avoid heterocoagulation. The synthesis of $C_{60}(PI)_n$, depending on the reaction conditions, produced multiadducts with n ranging from 2 to 5, including multiple regioisomers for each n. To avoid confusion, we will refer to $C_{60}(PI)_n$ with $n = 3$ to 5 as "higher" adducts and fullerenes with $n = 2$ as "mixed-bis" adducts.

We achieved control over the solution-phase aggregation of these materials by exploiting the different solubility properties of the conjugated polyelectrolyte and charged fullerene derivatives. Mixed-bis adducts show limited solubility (without PFT) in aqueous solution, whereas higher adducts are water soluble at high concentration. This difference suggests that the mixed-bis adducts should coassemble in aqueous solution with PFT, a result we confirmed by cryogenic electron microscopy (cryoEM), small-angle x-ray scattering (SAXS), and luminescence quenching studies. CryoEM images of pure PFT, PFT:mixed-bis adducts, and PFT:high adducts

[1]Department of Chemistry and Biochemistry, University of California–Los Angeles (UCLA), Los Angeles, CA 90095-1569, USA. [2]Department of Microbiology, Immunology and Molecular Genetics, and the Biomedical Engineering Program, UCLA, Los Angeles, CA 90095, USA. [3]The California NanoSystems Institute (CNSI), UCLA, Los Angeles, CA 90095, USA. [4]Department of Materials Science and Engineering, UCLA, Los Angeles, CA 90095, USA.
*These authors contributed equally to this work. †**Corresponding author. E-mail: tolbert@chem.ucla.edu (S.H.T.), schwartz@chem.ucla.edu (B.J.S.), rubin@chem.ucla.edu (Y.R.)**

Downloaded from www.sciencemag.org on June 19, 2015

are shown in Fig. 1, D to F. Pure PFT samples self-assemble into branched micelles that are roughly 4 ± 0.5 nm in diameter and 30 to 50 nm in length. CryoEM images of PFT assembled with mixed-bis adducts are visually similar to the pure PFT, indicating association of the $C_{60}(PI)_2$ with the PFT micelles. In contrast, cryoEM images of PFT:high adducts appear blurry because these solutions contain separate PFT and fullerene agglomerates.

This interpretation of coassembly of PFT with mixed-bis adducts is also supported by SAXS measurements (Fig. 2, A and B). We radially averaged the SAXS data and fit it to a power law to extract the exponent α, which is related to the polymer fractal structure (*12*, *13*). Values of α = 1, 2, and 4 correlate to rigid rod, lamellar, and spherical structures, respectively, although interactions between molecules cause deviations from these ideal slopes. Analysis of SAXS data for pure PFT yielded α = 1.5 at low *q* (rod-like at large size), increasing to α = 3.7 at high *q* (sphere-like at small size). Deviation from α = 1 arose from the branched network seen by cryoEM (Fig. 1D) (*14*). SAXS power-law slopes for $C_{60}(PI)_n$ high-adducts correspond to a percolation network at low *q* and rod-like behavior at high *q*, indicating aggregation (*12*, *15*). SAXS data from the combined PFT:high adducts solution was well approximated as the mass-scaled sum of the pure PFT and pure fullerene scattering, suggesting a nonassembled mixture, similar to that seen by cryoEM. By contrast, mass-scaled SAXS from solutions of PFT and mixed-bis adducts is nearly identical to the pure PFT. These results provide strong evidence that $C_{60}(PI)_2$ and PFT coassemble into a single micellar aggregate.

Finally, electronic interactions in the polymer-fullerene assemblies were confirmed with luminescence quenching, which provides an indirect measure of the photoinduced charge transfer from the polymer to the fullerenes (*16*). Solutions of PFT:high adducts showed relatively little photoluminescence (PL) quenching, presumably because the donors and acceptors were not in close physical proximity, but aqueous solutions of PFT with the mixed-bis adducts had substantial PL quenching, indicating both physical and electronic contact (Fig. 3A). The data indicate that >75% of the PFT excitations were quenched in the presence of the mixed-bis adducts.

We determined the dynamics of charge separation in these donor-acceptor assemblies using ultrafast broadband transient absorption spectroscopy on dilute aqueous solutions of coassembled PFT with mixed-bis adducts (*17*). Representative transient absorption spectra at different probe delays following excitation at 470 nm are shown in Fig. 3B. We assigned the negative transient absorption peak near 520 nm to stimulated emission, as the spectral features and the lifetime (Fig. 3C) matched the fluorescence emission. Interestingly, the 690-nm absorption of the PFT hole polaron (P^+) appeared on a subpicosecond time scale after photoexcitation (*18*, *19*). This ultrafast appearance of P^+ confirmed that the $C_{60}(PI)_2$ adducts must be coassembled with PFT, because other geometries would require diffusion or other structural rearrangements that could not occur so quickly. Once formed, about 75% of the PFT polarons in these dilute samples decayed back to the ground state in ~200 ps (Fig. 3C). The remaining polarons survived past the nanosecond time scale.

To mimic biological charge-separation systems, coassembly and rapid charge separation are required, but if they are followed by rapid recombination, the charges cannot be extracted. A fullerene acceptor that is optimized for charge separation thus needs to contain one class of compounds that can assemble intimately with the PFT for efficient charge transfer, and a second class of compounds that can assemble more loosely, allowing us to pull the electron away from the PFT and prevent recombination. Fortunately, both types of compounds were already available within our mixed-bis sample, and their properties could be examined simply by separating $C_{60}(PI)_2$ regioisomers. Our mixed-bis samples were primarily composed of four isomers (10% *trans*-1, 39% *trans*-2, 44% *trans*-3,

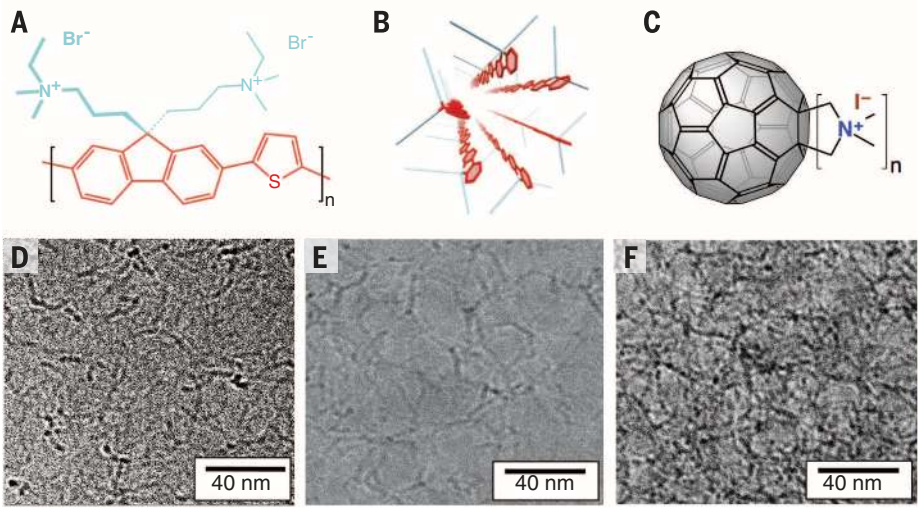

Fig. 1. PFT and charged fullerene structure and assembly. PFT structure (**A**); cartoon of a PFT micelle (**B**); charged fullerenes (**C**). CryoEM images of pure PFT (**D**), PFT:mixed-bis adducts (**E**), and PFT:high adducts (**F**).

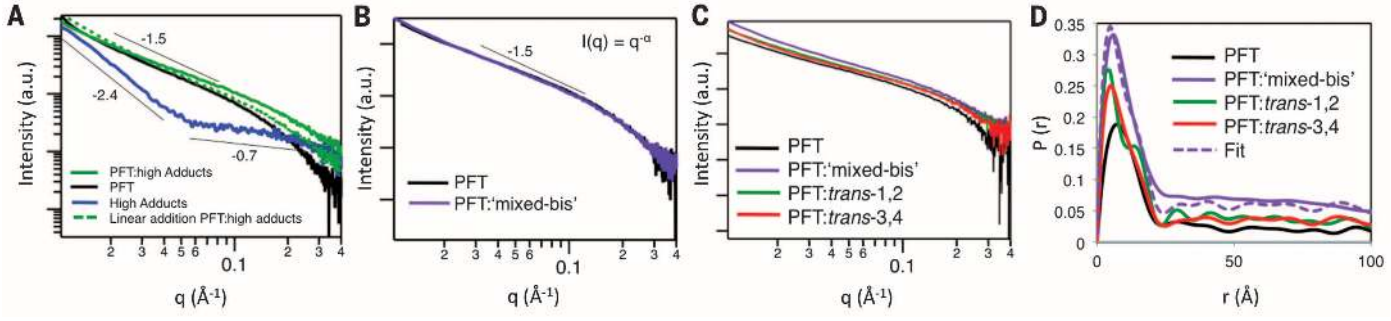

Fig. 2. SAXS data for PFT and PFT/fullerene mixtures. (**A**) Data for PFT:high-adducts are reasonably approximated by a sum of PFT + high-adducts. (**B**) The PFT:mixed-bis profile overlap mass-scaled PFT data. (**C**) Raw scattering data for all PFT and PFT:bis-fullerene samples are similar. (**D**) Distance distribution functions, *P*(*r*), obtained by Fourier transformation of the data in (C) show different fullerene environments for *trans*-1,2 and *trans*-3,4, with PFT:mix-bis corresponding to the sum of the two.

and 7% *trans*-4). Structures of each of the isomers are shown in Fig. 4, A to D. We partially separated these isomers by silica gel column chromatography of the neutral pyrrolidine precursors (prior to quaternization), producing fractions that we refer to as *trans*-1,2 (29% *trans*-1 and 71% *trans*-2) and *trans*-3,4 (14% *trans*-2, 74% *trans*-3, and 12% *trans*-4). The full characterization of all of these materials is found in figs. S1 to S22 of the supplementary materials (*17*). The *trans*-1,2 fullerenes have charges on nearly opposite sides of the buckyball and can be viewed as isotropically charged molecules that should not easily insert into a PFT micelle. By contrast, the angle between charges in *trans*-3 is ~145° and that between charges in *trans*-4 is 103°, suggesting more amphiphilic molecules that could insert into the PFT micelle.

The coassembly of PFT with *trans*-1,2 and *trans*-3,4 was examined via SAXS. Raw scattering data for all of the samples looked similar to the data for pure PFT (Fig. 2C), but Fourier analysis using cylindrical boundary conditions showed subtle variations. In Fig. 2D, PFT and PFT:*trans*-3,4 showed similar probability distributions, supporting the model of insertion of fullerene into the PFT micelle. PFT:*trans*-1,2 shows two peaks, reminiscent of a polymer micelle with a partial "shell" of fullerenes surrounding the outside. The PFT:mixed-bis data were well fit by a simple linear combination of the PFT:*trans*-1,2 and PFT:*trans*-3,4 probability distributions, further supporting the idea that *trans*-3,4 assembles on the inside of the polymer micelle, whereas *trans*-1,2 surrounds the outside. The relative locations of the two different sets of fullerenes were also confirmed via solvatochromic absorption measurements (fig. S25). These measurements show that the ultraviolet absorption of *trans*-1,2 fullerenes assembled with PFT matches that of the fullerenes in pure water, indicating that *trans*-1,2 sits outside of the PFT micelle. In contrast, the absorption of the *trans*-3,4 fullerenes assembled with PFT matches that of the fullerenes in organic solvents, indicating that *trans*-3,4 sits in a lower dielectric environment like the micelle interior.

Figures 4, F and G, show luminescence quenching measurements that further support the idea that different isomers of $C_{60}(PI)_2$ assemble in different places in the PFT micelle. The luminescence decays shown in Fig. 4G were taken with a Kerr-gated time-resolved fluorescence setup using CS_2 as the gate medium, providing a time resolution of ~1 ps (*20*). Clearly, the PFT fluorescence is quenched nearly to the instrument limit in concentrated solutions when assembled with *trans*-3,4 fullerenes, verifying that the photoinduced charge transfer to these fullerenes is ultrafast. In contrast, there is almost no fast quenching of the PFT emission with an equal amount of *trans*-1,2 fullerenes, reflecting their assembled position predominantly on the outside of the micelle, out of range for fast ET. Figure 4F shows steady-state luminescence measurements on these same samples. Consistent with the time-resolved data, assemblies of PFT with *trans*-1,2 fullerenes showed little luminescence quenching, whereas PFT assembled with *trans*-3,4 fullerenes had strong quenching. These quenching results suggested that not only can we selectively associate fullerenes with polymer micelles using the number of charges, we can also control the position of the fullerene within the micelle by the placement of the charges (Fig. 4E).

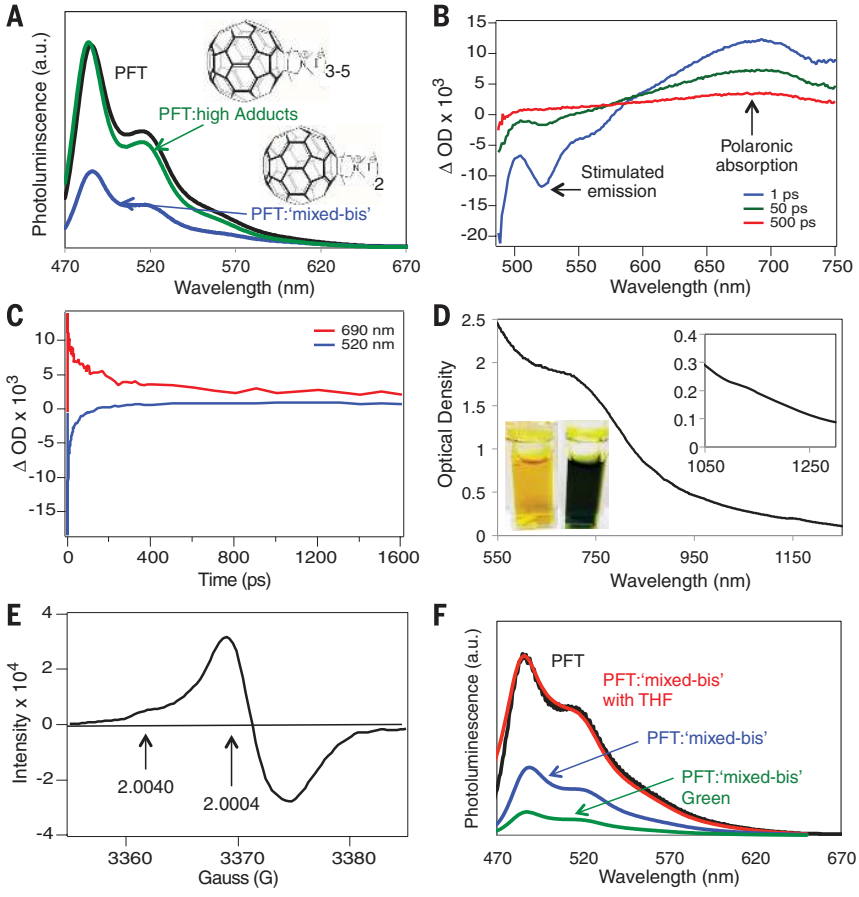

Fig. 3. Formation of P^+ and N^- polarons requires intimate assembly of the polymer and fullerene. (**A**) PL of PFT, PFT:high adducts, and PFT:mixed-bis; (**B**) pump-probe spectroscopy for dilute PFT:mixed-bis solutions excited at 470 nm showing the rapid formation of both excitons and polarons; (**C**) time decays for the stimulated emission and the polaronic absorption from (B). Absorption from a green concentrated PFT/fullerene solution showing both P^+ and N^- polarons (**D**). EPR from a similar green solution, again showing both P^+ and N^- polarons (**E**). PL for various concentrated PFT:mixed-bis solutions showing that polarons quench luminescence, but the addition of THF, which, destroys the PFT/fullerene assembly, restores PL intensity (**F**).

Given this degree of control, the next step was to examine long-lived excitations in assemblies of PFT and mixed-bis adducts containing both intimately assembled *trans*-3,4 and more isotropically charged *trans*-1,2 fullerenes. Ideally, this coassembly should permit rapid photoinduced electron transfer from PFT to the *trans*-3,4 fullerenes, followed by a second ET step to the *trans*-1,2 fullerenes. If this type of directed ET cascade occurs, electrons on the *trans*-1,2 fullerenes would then be stabilized in the high-dielectric environment of the water surrounding the micelle, preventing recombination with the PFT. Indeed, we found that photoexcitation of aqueous PFT:mixed-bis adduct solutions caused a dramatic color change from yellow to dark green over time (Fig. 3D); once the solution was exposed to light, the color change was essentially permanent, lasting days to weeks. Dilute solutions, like those used to collect the data in Fig. 3, B and C, required extensive light exposure (fig. S24), but when higher concentrations were used, the color change took place in just a few seconds under room lights, indicating that the quantum yield for long-lived charge separation is much higher than the ~25% in dilute solutions (compare Fig. 3B).

PFT is a blue-absorbing polymer with an absorption maximum at 430 nm in water and little to no absorbance above 550 nm (*10*). The color change from yellow to green was confirmed to arise from the appearance of the PFT hole polaron (P^+) by comparing steady-state data (Fig. 3D) with transient absorption data (Fig. 3B) and absorption from PFT oxidized with iodine, both of which show absorption in the sub-gap region

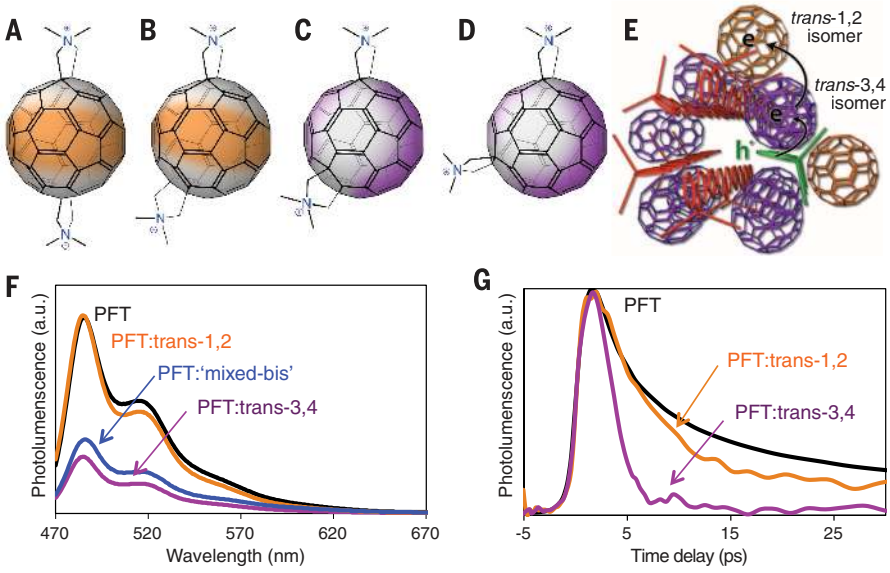

Fig. 4. Spectroscopic evidence for long-lived charged species in solution. Chemical structures of *trans*-1 bis (**A**), *trans*-2 bis (**B**), *trans*-3 bis (**C**), and *trans*-4 bis (**D**) fullerene derivatives with color emphasizing the hydrophobic regions. Cartoon depicting the assembly of *trans*-1,2 (orange) and *trans*-3,4 (purple) bis fullerenes with PFT (red). Photoexcitation of the PFT backbone leads to charge transfer first to *trans*-3,4 and then to *trans*-1,2, where the electron remains due to stabilization by the reorganization of water. The hole (green, h^+) remains on PFT (**E**). PL of PFT, PFT:mixed-bis, PFT:*trans*-3,4 bis, and PFT:*trans*-1,2 bis (**F**). Time-resolved luminescence for assembled concentrated PFT:*trans*-3,4 bis and PFT:*trans*-1,2 bis samples (**G**).

at ~690 nm (fig. S23) (*21*). The Fig. 3D inset shows that simultaneously, a substantially weaker negative (N^-) polaron absorption peak caused by the $C_{60}(PI)_2$ molecular anion was observed at 1180 nm. The low intensity of the N^- absorption has several origins: (i) The absorption cross-section of fullerene anions is much smaller than that of the polymer polarons (*22*); (ii) the weak N^- absorption peak sits on top of a broad scattering background from the coassembled micelles in solution; and (iii) the N^- polaron might react with impurities in the water, despite our best efforts to deoxygenate the solutions by freeze-pump-thaw techniques (*23*).

To further confirm the formation of stable, separated N^- and P^+ polarons after exposure to light, we performed electron paramagnetic resonance (EPR) experiments. Figure 3E shows the EPR signal from the green PFT:mixed-bis adducts solution; the *g*-factors for the N^- and P^+ polarons are 2.0004 and 2.0040, respectively, in good agreement with reported values for many other polymer-fullerene systems (*24*). The N^- polaron line width that we observed is broader than that in other polymer-fullerene systems, both because of the interaction of the water dipoles with the polarons and because of different spin-relaxation times for the electron and hole (*25*, *26*). The critical difference between our coassembled system and previous systems, however, is that the previous EPR work required active photoexcitation (light-induced EPR) in order to observe the polaron signals. In contrast, once exposed to light, the polarons created in our PFT:$C_{60}(PI)_2$ solutions remained stable essentially indefinitely.

Final confirmation that the long-lived separated charges resulted from a self-assembled ET cascade comes by examining the details of absorption and luminescence for a range of samples in different solvents. As discussed above, aqueous solutions of PFT and *trans*-1,2 fullerenes show little PL quenching (Fig. 4, F and G), but they did briefly turn green during the course of the dissolution, indicating polaron formation (possibly from disordered polymer that transiently allowed the fullerene to partly insert into the micelle). By contrast, despite the efficient luminescence quenching in solutions of PFT coassembled with the *trans*-3,4 fullerenes (Fig. 4, F and G), the solutions did not turn green and ultrafast experiments (data not shown) indicate that polarons are formed on subpicosecond time scales (as in Fig. 3B), but recombine with 100% yield over the next few hundred picoseconds. These results indicate that controlling the spatial position of the fullerenes can dramatically affect carrier dynamics. Moreover, photoexcitation of green-colored PFT:mixed-bis fullerene solutions results in increased luminescence quenching because PFT excitons are further quenched by P^+-polarons (Fig. 3F). However, when tetrahydrofuran (THF), which is known to disassemble the polymer micelles (*27*), was added to the coassembled green system, the luminescence signal regained its intensity, indicating a fully reversible system (Fig. 3F). These results further support the idea that intimate assemblies with well-controlled molecular positions are required to facilitate a charge transfer cascade and avoid recombination. When nanoscale architecture is optimized, the result is stable polarons that could potentially be applied to improve organic photovoltaic cells via suppression of charge recombination.

REFERENCES AND NOTES

1. A. W. Rutherford, *Trends Biochem. Sci.* **14**, 227 (1989).
2. J. Piris *et al.*, *J. Phys. Chem. C* **113**, 14500 (2009).
3. P. E. Shaw, A. Ruseckas, I. D. W. Samuel, *Adv. Mater.* **20**, 3516 (2008).
4. S. Gélinas *et al.*, *J. Phys. Chem. C* **115**, 7114 (2011).
5. J. Verhoeven, *J. Photochem. Photobiol. Photochem. Rev.* **7**, 40 (2006).
6. T. Miura, K. Maeda, H. Murai, T. Ikoma, *J. Phys. Chem. Lett.* **6**, 267 (2015).
7. C. Lungenschmied *et al.*, *Sol. Energy Mater. Sol. Cells* **91**, 379 (2007).
8. T. Yasuda, Y. Shinohara, T. Ishi-i, L. Han, *Org. Electron.* **13**, 1802 (2012).
9. T. Costa *et al.*, *J. Phys. Chem. B* **118**, 613 (2014).
10. A. P.-Z. Clark *et al.*, *ACS Nano* **7**, 962 (2013).
11. A. Cassell, C. Asplund, J. Tour, *Angew. Chem.* **38**, 2403 (1999).
12. G. Beaucage, *J. Appl. Cryst.* **29**, 134 (1996).
13. S. Choudhary, S. R. Bhatia, *Carbohydr. Polym.* **87**, 524 (2012).
14. Y.-C. Li *et al.*, *Langmuir* **22**, 11009 (2006).
15. U. Jeng *et al.*, *Nucl. Instrum. Methods Phys. Res. A* **600**, 294 (2009).
16. Y. Park *et al.*, *Polymer (Guildf.)* **55**, 855 (2014).
17. See supplementary materials on *Science* Online for details.
18. R. Österbacka, C. P. An, X. M. Jiang, Z. V. Vardeny, *Science* **287**, 839 (2000).
19. F. Paquin *et al.*, *Phys. Rev. Lett.* **106**, 197401 (2011).
20. S. Arzhantsev, M. Maroncelli, *Appl. Spectrosc.* **59**, 206 (2005).
21. C. Chiang *et al.*, *Phys. Rev. Lett.* **39**, 1098 (1977).
22. T. Kato *et al.*, *Chem. Phys. Lett.* **186**, 35 (1991).
23. D. M. Guldi, M. Prato, *Acc. Chem. Res.* **33**, 695 (2000).
24. V. I. Krinichnyi, *Sol. Energy Mater. Sol. Cells* **92**, 942 (2008).
25. T. J. Savenije *et al.*, *Phys. Chem. Chem. Phys.* **13**, 16579 (2011).
26. J. Ceuster, E. Goovaerts, A. Bouwen, J. C. Hummelen, V. Dyakonov, *Phys. Rev. B* **64**, 195206 (2001).
27. E. G. Kelley, T. P. Smart, A. J. Jackson, M. O. Sullivan, T. H. Epps 3rd, *Soft Matter* **7**, 7094 (2011).

ACKNOWLEDGMENTS

This work was supported by the NSF under grant CHE-1112569 and by the Center for Molecularly Engineered Energy Materials, an Energy Frontier Research Center funded by the U.S. Department of Energy (DOE) under Contract DE-AC06-76RLO-1830. A.S.F acknowledges support from The Clean Green IGERT (NSF DGE-0903720). This work made use of facilities support by the NSF under equipment grant CHE-1048804. Portions of this work were conducted at the Stanford Synchrotron Radiation Lightsource (SSRL), which is supported under DOE Contract DE-AC02-76SF00515. The SSRL Structural Molecular Biology Program is supported by the DOE Office of Biological and Environmental Research and by the National Institutes of Health, National Institute of General Medical Sciences (including P41GM103393). We acknowledge the use of instruments at the Electron Imaging Center for NanoMachines supported by the NIH (1S10RR23057 to Z.H.Z.) and CNSI at UCLA.

SUPPLEMENTARY MATERIALS

www.sciencemag.org/content/348/6241/1340/suppl/DC1
Materials and Methods
Figs. S1 to S25
References (*28*–*31*)

14 January 2015; accepted 21 May 2015
10.1126/science.aaa6850